histological grade ($P = 0.0465$) and vascular invasion ($P = 0.0326$); however, there were no statistically significant differences in histology, age, gender, size, lymph node metastasis, or neural invasion (Table 1).

Protein expression of actinin-4 determined by IHC

We investigated the protein expression level of actinin-4 by using IHC. Among the 58 tumors, 14 (24.1%) had strong (+3) expression, 25 (43.1%) had moderate (+2) expression, 13 (22.4%) had weak (+1) expression, and six (10.3%) had no (0) expression.

Positive staining for actinin-4 protein, which was defined as moderate expression (+2) and strong expression (+3), occurred in 39 of 58 tumors (67.2%) (Fig. 1E–H). The distribution of actinin-4 protein in histological subtypes is described in Table 1. There were no statistically significant differences between the positive and negative staining groups in terms of age, gender, size, lymph node metastasis, histological grade, neural invasion, or vascular invasion (Table 1).

In normal submandibular salivary glands, actinin-4 proteins were equally expressed in acinar cells, intercalated duct cells, striated duct cells and endothelial cells. In contrast, in the parotid gland, the protein expression level of actinin-4 in acinar cells was weaker than in ductal cells (Fig. 1C and D).

The correlation between copy number of *ACTN4* and protein expression of actinin-4

We confirmed the correlation between *ACTN4* copy number and protein expression of actinin-4. CNI of *ACTN4* was recognized in 12 of 39 (30.8%) tumors with positive staining of actinin-4. CNI was recognized in six of 14 (42.9%) tumors with strong (+3) expression of actinin-4, six of 25 (24.0%) tumors with moderate (+2) expression, and two of 19 (10.5%) tumors with negative (0 and +1) staining (Fig. 2A). Although 18 of 21 ADCCs were positively stained for actinin-4 (85.7%), CNI of *ACTN4* was recognized in only one ADCC (4.8%) (Fig. 2A). Therefore, we considered that the expression level of actinin-4 protein is not positively associated with CNI of *ACTN4* in ADCC. We then investigated the correlation between protein expression levels and copy number of *ACTN4* in salivary gland carcinomas excluding ADCCs. The average copy numbers of *ACTN4* in salivary gland carcinomas excluding ADCC were 5.12, 2.90, and 2.47 in tumors with strong expression (+3), moderate expression (+2), and negative staining (0 and +1), respectively. Copy numbers of *ACTN4* were significantly increased in tumors with strong expression (+3) of actinin-4 in comparison with negative staining (0 and +1) and moderate expression (+2) ($P < 0.01$) in salivary gland carcinomas, excluding ADCC (Fig. 2B).

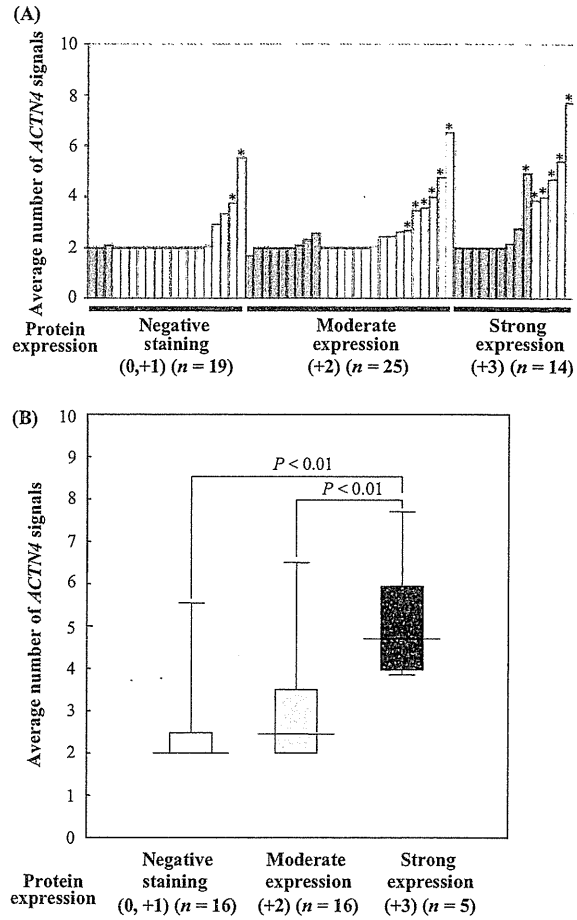

Figure 2. Collation between copy numbers of *ACTN4* and actinin-4 protein. (A) Bar graph of copy numbers of *ACTN4* in individual patients (*y*-axis; average number of *ACTN4* signals, gray bars; patients with adenoid cystic carcinoma (ADCC), white bars; patients with salivary gland carcinomas excluding ADCC, *; the patients with copy number increase [CNI]). (B) Box and whisker plot for average number of *ACTN4* signals between protein expression levels of actinin-4 proteins in the patients with salivary gland carcinomas excluding ADCC. The average number of *ACTN4* signals in the patients with strong expression of actinin-4 protein was significantly higher than the patients with moderate expression or negative staining of actinin-4 protein ($P < 0.01$, Student's *t*-test).

The prognostic significance of CNI of *ACTN4*

Kaplan–Meier analysis revealed that CNI of *ACTN4* was significantly correlated with poor outcome in overall survival of the 58 patients with salivary gland carcinoma,

including ADCC ($P = 0.0005$, log-rank test) (Fig. 3A). ADCC has a better prognosis than high-grade histological subtypes of salivary gland carcinoma [21]. The correlation analysis between CNI and protein expression in ADCC (Fig. 2A, gray bars) revealed that although 85.7% of ADCCs had strong expression (+3) or moderate expression (+2) of actinin-4 protein, CNI of *ACTN4* was recognized in only one tumor. To remove the bias of the unique prognosis of ADCC, we also investigated the prognostic significance with CNI of *ACTN4* in 37 salivary gland carcinoma patients excluding ADCC. A statistically significant difference in prognosis was recognized between patients with NCN and patients with CNI ($P = 0.0112$); the overall survival of patients with CNI was worse than patients with NCN (Fig. 3C). In contrast, the actinin-4 protein expression level was not statistically correlated to overall survival in salivary gland carcinomas when including or excluding ADCC (Fig. 3B and D).

HR for death in patients with salivary gland carcinoma

We calculated the hazard ratios (HR) of some parameters, including age, gender, size, lymph node metastasis, histological grade, neural invasion, vascular invasion, actinin-4 protein expression, and CNI of *ACTN4*, for death by using univariate and multivariate Cox regression analysis.

In the patients with salivary gland carcinomas including ADCC, histological grade (HR: 4.69; 95% confidence interval [CI]: 1.50–14.61), vascular invasion (HR: 10.86; 95% CI: 3.56–33.14), and CNI of *ACTN4* (HR: 5.21; 95% CI: 1.92–14.19) remained as positive predictors by using univariate analysis, and multivariate analysis revealed that vascular invasion (HR: 7.46; 95% CI: 1.98–28.06) and CNI of *ACTN4* (HR: 3.23; 95% CI: 1.08–9.68) were independent positive predictors for death in patients with salivary gland carcinoma (Table 2).

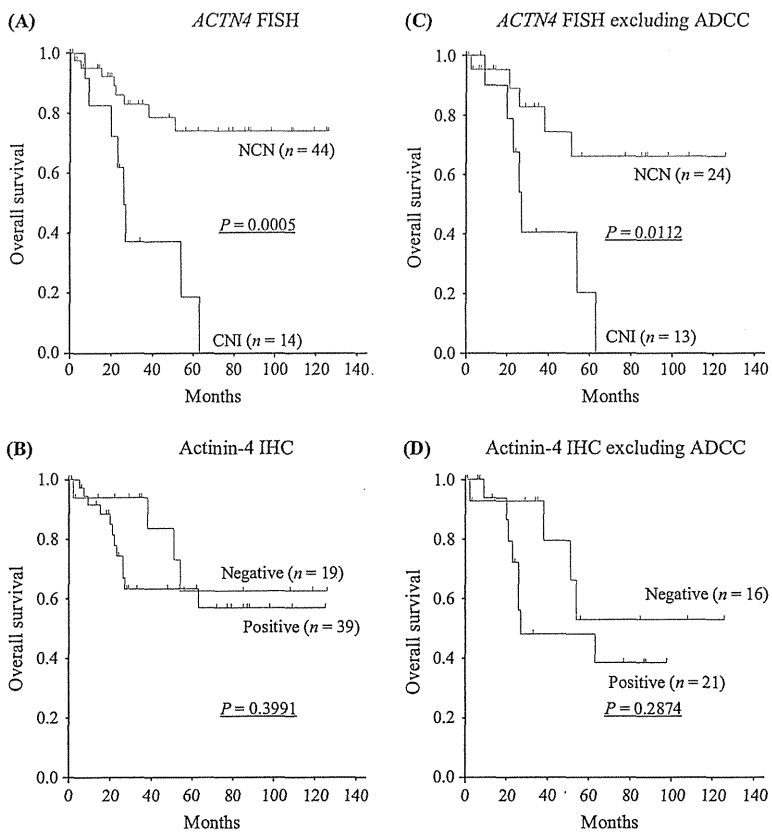

Figure 3. Overall survival curves of patients with salivary gland carcinomas, including adenoid cystic carcinoma (ADCC) (A and B) or excluding ADCC (C and D), by evaluations of fluorescence in situ hybridization (FISH) (A and C) or immunohistochemistry (IHC) (B and D). The statistical significances were recognized in evaluation of FISH between copy number increase (CNI) and normal copy number (NCN) in patients with salivary gland carcinomas including/excluding ADCC (A and C). In contrast, the statistical significance was not recognized in an evaluation of IHC in both cohorts (B and D).

Table 2. Hazard ratios for death in salivary gland cancer patients.

	Univariate analysis[1]			Multivariate analysis[1]		
Variable	HR	95% CI	*P*-value	HR	95% CI	*P*-value
Age						
<67/≥67 years	2.69	0.93–7.78	0.067			
Gender						
Women/men	1.20	0.45–3.24	0.714			
T classification						
T1–T2/T3–T4	2.28	0.51–10.11	0.279			
Lymph node metastasis						
Absent/present	2.51	0.93–6.75	0.069			
Histological grade						
Low, intermediate/high	4.69	1.50–14.61	**0.007765**	1.32	0.31–5.45	0.701222
Neural invasion						
Absent/present	1.38	0.51–3.71	0.524			
Vascular invasion						
Absent/present	10.86	3.56–33.14	**0.000028**	7.46	1.98–28.06	**0.002958**
Actinin-4 IHC						
Negative/positive	1.64	0.53–5.10	0.394			
ACTN4 FISH						
NCN/CNI	5.21	1.92–14.19	**0.001230**	3.23	1.08–9.68	**0.035815**

HR, hazard ratio; CI, confidence interval; FISH, fluorescent in situ hybridization; IHC, immunohistochemistry; NCN, normal copy number; CNI, copy number increase.

[1]Univariate and multivariate analysis with Cox proportional hazards regression model. *P*-values of <0.05 are shown in bold.

We also calculated the HRs for death in patients with salivary gland carcinomas excluding ADCC. Univariate analysis revealed that vascular invasion (HR: 8.58; 95% CI: 2.16–34.11) and CNI of *ACTN4* (HR: 4.18; 95% CI: 1.29–13.53) were significant positive predictors for death in salivary gland carcinomas excluding ADCC. Multivariate analysis also revealed that vascular invasion and CNI of *ACTN4* were independent risk factors for both salivary gland carcinomas including and excluding ADCC (Table 3).

Discussion

The assessment of prognostic factors in salivary gland carcinoma is difficult due to its low frequency and morphological diversity [22]. Histological grading of salivary gland carcinoma is an important predictor of survival [23]. It can stratify the risk of lymph node metastases and provide information for deciding the treatment strategy, including the extent of surgery and the use of adjuvant radiotherapy [24]. In the present study, we identified a novel predictor for the prognosis of salivary gland carcinoma and found that it was significantly associated with histological grade.

Our laboratory identified the *ACTN4* gene product as an actin-bundling protein that was closely associated with cell movement and cancer invasion [3]. In a previous study, colorectal cancer cell lines in which actinin-4 was overexpressed stimulated invasive cellular protrusions and had a significantly more invasive phenotype than control cells [4]. Moreover, pancreatic and oral squamous cell carcinoma cells in which actinin-4 expression was reduced with siRNA exhibited decreased invasiveness [10, 11]. An orthotopic transplantation study of cells overexpressing actinin-4 revealed that the regional lymphatic metastasis and destructive invasion to stromal cells were significantly increased in colorectal [4] and pancreatic cancer [11].

Actinin-4 overexpression was also confirmed in solid malignant tumors that had been surgically excised, and protein expression was an unfavorable predictor of patient outcome. One cause of actinin-4 protein overexpression is *ACTN4* gene amplification. In fact, gene amplification of *ACTN4* has been detected in tumors from patients with pancreatic [11], ovarian [6, 7], and lung cancers [13], and correlations between protein expression and gene amplification have been statistically recognized in some cancers. Especially, Noro et al. reported that *ACTN4* amplification could more strictly predict poor outcome than actinin-4 protein expression in stage-I adenocarcinoma of the lung [13]. To identify the specificity of gene amplification of *ACTN4*, we previously examined the correlation of gene amplification of a gene near *ACTN4*. V-akt murine thymoma viral oncogene homolog 2 (*AKT2*) is located on 19q13, and it is near *ACTN4*. The distance between *ACTN4* and *AKT2* is 1.6 Mbp. We previously reported that coamplification of

Table 3. Hazard ratios for death in salivary gland cancer patients excluding ADCC.

	Univariate analysis[1]			Multivariate analysis[1]		
Variable	HR	95% CI	*P*-value	HR	95% CI	*P*-value
Age						
<67/≥67 years	2.52	0.68–9.41	0.1688			
Gender						
Women/men	2.10	0.57–7.82	0.2670			
T classification						
T1–T2/T3–T4	1.68	0.36–7.81	0.5075			
Lymph node metastasis						
Absent/present	1.55	0.50–4.83	0.4483			
Histological grade						
Low, intermediate/high	2.81	0.76–10.44	0.1228			
Neural invasion						
Absent/present	1.50	0.47–4.72	0.4932			
Vascular invasion						
Absent/present	8.58	2.16–34.11	**0.0023**	9.00	2.15–37.61	**0.0026**
Actinin-4 IHC						
Negative/positive	1.91	0.57–6.43	0.2912			
ACTN4 FISH						
NCN/CNI	4.18	1.29–13.53	**0.0168**	4.35	1.28–14.87	**0.0187**

ADCC, adenoid cystic carcinoma; HR, hazard ratio; CI, confidence interval; FISH, fluorescent in situ hybridization; IHC, immunohistochemistry; NCN, normal copy number; CNI, copy number increase.

[1]*Univariate and multivariate analysis with Cox proportional hazards regression model. P-values of <0.05 are shown in bold.*

AKT2 and *ACTN4* did not necessarily accord for invasion of pancreatic cancer [5, 11]. The present study is the first report that CNI of *ACTN4*, including gene amplification and high polysomy of *ACTN4*, was significantly correlated to histological grade and vascular invasion in salivary gland carcinoma. CNI of *ACTN4* was recognized at a frequency greater than 20% in OC (1/1, 100%), MYC (1/1, 100%), SC (2/3, 66.7%), SDC (2/4, 50.0%), EMYC (1/3, 33.3%), ACNOS (2/7, 28.6%), CAEPA (3/11, 27.3%), and MEC (1/4, 25.0%). However, CNI of *ACTN4* was not found in patients with acinic cell carcinoma (ACCC) (0/3, 0%) and was rarely observed in patients with ADCC (1/21, 4.8%). The survival time of the patient with CNI of *ACTN4* in ADCC was 7 months from the first treatment. Despite the rare frequency of CNI of *ACTN4* in ADCC, overexpression of actinin-4 protein was recognized in 85.7% of patients with ADCC. ADCC has several cellular components constructed by ductal epithelial, myoepithelial, and basement cells, and protein expression of actinin-4 is particularly recognized in myoepithelial cells of normal salivary glands. Therefore, it was considered that the protein expression of actinin-4 was dependent on the histological phenotype; however, this was not associated with the genetic alteration that was dependent on malignant change.

-ADCC was different from other subtypes of salivary gland carcinomas, we investigated the correlation between CNI and protein expression of actinin-4 by using 37 patients with salivary gland carcinomas excluding ADCC. Significant correlations were recognized between increased copy numbers of *ACTN4* and protein expression levels of actinin-4. This data suggests that the overexpression of actinin-4 protein was stimulated by CNI of *ACTN4*. Cox regression univariate analysis revealed that histological grade, vascular invasion, and CNI of *ACTN4* were risk factors for cancer death in salivary gland carcinoma patients with or without ADCC. The HR of CNI of *ACTN4* for death was higher than the HR for the histological grade. In addition, although multivariate analysis revealed that CNI of *ACTN4* and vascular invasion were independent risk factors for tumor death, histological grade did not remain as an independent risk factor. These results suggest that CNI of *ACTN4* may have a greater impact than histological grade on patient death. Although CNI of *ACTN4* was significantly correlated with histological grade and vascular invasion, the protein expression of actinin-4 was not associated with any clinical factors in salivary gland carcinoma. In addition, protein expression could not predict an unfavorable outcome in patients with salivary gland carcinoma. Although CNI of *ACTN4* was dominantly recognized in salivary gland carcinoma with invasive phenotypes, it was recognized in only one of 21 cases with ADCC; therefore, we considered the possibility that, due to the overexpression of actinin-4 that was frequently observed in ADCC patients, protein expression is not correlated to an unfavorable prognosis in salivary gland carcinoma. In contrast,

protein expression of actinin-4 was recognized in 18 cases with ADCC. An explanation for this observation involved the discrepancy between CNI and protein expression of actinin-4 in ADCC. We analyzed the correlation between overall survival and protein expression of actinin-4 in patients excluding ADCC; although statistical significance was not recognized, it seemed that overall survival in the positive staining group had a poorer prognosis than in the negative staining group. To probe the statistical significance of protein expression of actinin-4, we considered that the power of statistical hypothesis testing was not enough. More non-ADCC salivary gland carcinoma samples are needed to prove a significant correlation between overall survival and protein expression. Moreover, although CNI can quantitatively evaluate the copy numbers of the *ACTN4* gene, our evaluation system for protein expression of actinin-4 cannot quantitatively classify the cases with protein expression of actinin-4. Therefore, we considered that CNI of *ACTN4* more strictly predicted the vascular invasion of cancer cells and poor prognosis than protein expression of actinin-4. Similar observations have also been recognized in ovarian cancer. We previously reported that the gene amplification of *ACTN4* could predict the prognosis of patients with advanced stage ovarian cancer more accurately than protein expression of actinin-4 [6].

Ettl et al. reported the occurrence of genomic aberrations of the tyrosine kinase receptors *EGFR*, human epidermal growth factor receptor 2 (*HER2*), and hepatocyte growth factor (*MET*) as well as phosphatase and tensin homolog on chromosome 10 (*PTEN*) in different subtypes of salivary gland carcinomas [25, 26], which have a strong impact on overall survival [27]. In addition, they also reported that the metastasis of cervical lymph nodes also correlated with copy number gain of *EGFR* and *HER2*, aberration of *MET*, and *PTEN* [20]. Moreover some translocation and fusion genes are found frequently in MEC t(11;19) (CRYC1-MAML2) [28] or ADCC t(6;9) (MYB-NFIB) [29] and have a prognostic impact. These genetic alterations are considered as a driver for malignant phenotype, and molecular-targeted therapy has gained attention as a new therapeutic strategy for salivary gland carcinomas. In fact, clinical trials with some inhibitors or antibodies for molecular targets, such as gefitinib (a small-molecule *EGFR* inhibitor), cetuximab (an anti-EGFR antibody), and trastuzumab (an anti-HER2 antibody), were performed for patients with salivary gland carcinomas. Although the results of phase II clinical trials of gefitinib, cetuximab, and trastuzumab have been reported [30, 31], standard molecular-targeted therapy has not yet been established for salivary gland carcinoma.

ACTN4 is located on chromosome 19q13.1 [11]. Genetic alterations of 19q13.1 and *ACTN4* have not yet been reported in salivary gland carcinoma. Although a large-scale prospective study to prove the clinical significance for *ACTN4* is necessary, we conclude that *ACTN4* is a surrogate biomarker for predicting prognosis to support histological grading in salivary gland carcinoma and that the inhibition of the biological function of *ACTN4* may impact a new therapeutic strategy for high-grade salivary gland carcinoma.

Acknowledgment

This work was supported by a Grant-in Aid for Scientific Research (B) and a Challenging Exploratory Research from the Ministry of Education, Culture, Sports, Science and Technology (METX) of Japan (K. H.), and the National Cancer Center Research and Development Fund (23-A-38, and 23-A-11) (K. H.). We thank N. Miura, T. Watanabe, and T. Umaki for helpful discussions.

Conflict of Interest

None declared.

References

1. Speight, P. M., and A. W. Barrett. 2002. Salivary gland tumours. Oral Dis. 8:229–240.
2. Terhaard, C. H., H. Lubsen, I. Van der Tweel, F. J. Hilgers, W. M. Eijkenboom, H. A. Marres, et al. 2004. Salivary gland carcinoma: independent prognostic factors for locoregional control, distant metastases, and overall survival: results of the Dutch head and neck oncology cooperative group. Head Neck 26:681–692; discussion 692-683.
3. Honda, K., T. Yamada, R. Endo, Y. Ino, M. Gotoh, H. Tsuda, et al. 1998. Actinin-4, a novel actin-bundling protein associated with cell motility and cancer invasion. J. Cell Biol. 140:1383–1393.
4. Honda, K., T. Yamada, Y. Hayashida, M. Idogawa, S. Sato, F. Hasegawa, et al. 2005. Actinin-4 increases cell motility and promotes lymph node metastasis of colorectal cancer. Gastroenterology 128:51–62.
5. Hayashida, Y., K. Honda, M. Idogawa, Y. Ino, M. Ono, A. Tsuchida, et al. 2005. E-cadherin regulates the association between beta-catenin and actinin-4. Cancer Res. 65:8836–8845.
6. Yamamoto, S., H. Tsuda, K. Honda, K. Onozato, M. Takano, S. Tamai, et al. 2009. Actinin-4 gene amplification in ovarian cancer: a candidate oncogene associated with poor patient prognosis and tumor chemoresistance. Mod. Pathol. 22:499–507.
7. Yamamoto, S., H. Tsuda, K. Honda, M. Takano, S. Tamai, I. Imoto, et al. 2012. ACTN4 gene amplification and actinin-4 protein overexpression drive tumour development and histological progression in a high-grade

subset of ovarian clear-cell adenocarcinomas. Histopathology 60:1073–1083.
8. Yoshii, H., K. Ito, T. Asano, A. Horiguchi, and M. Hayakawa. 2013. Increased expression of alpha-actinin-4 is associated with unfavorable pathological features and invasiveness of bladder cancer. Oncol. Rep. 30:1073–1080.
9. Koizumi, T., H. Nakatsuji, T. Fukawa, S. Avirmed, T. Fukumori, M. Takahashi, et al. 2010. The role of actinin-4 in bladder cancer invasion. Urology 75:357–364.
10. Yamada, S., S. Yanamoto, H. Yoshida, I. Yoshitomi, G. Kawasaki, A. Mizuno, et al. 2010. RNAi-mediated down-regulation of alpha-actinin-4 decreases invasion potential in oral squamous cell carcinoma. Int. J. Oral Maxillofac. Surg. 39:61–67.
11. Kikuchi, S., K. Honda, H. Tsuda, N. Hiraoka, I. Imoto, T. Kosuge, et al. 2008. Expression and gene amplification of actinin-4 in invasive ductal carcinoma of the pancreas. Clin. Cancer Res. 14:5348–5356.
12. Welsch, T., S. Keleg, F. Bergmann, S. Bauer, U. Hinz, and J. Schmidt. 2009. Actinin-4 expression in primary and metastasized pancreatic ductal adenocarcinoma. Pancreas 38:968–976.
13. Noro, R., K. Honda, K. Tsuta, G. Ishii, A. M. Maeshima, N. Miura, et al. 2013. Distinct outcome of stage I lung adenocarcinoma with ACTN4 cell motility gene amplification. Ann. Oncol. 24:2594–2600.
14. Miyanaga, A., K. Honda, K. Tsuta, M. Masuda, U. Yamaguchi, G. Fujii, et al. 2013. Diagnostic and prognostic significance of the alternatively spliced ACTN4 variant in high-grade neuroendocrine pulmonary tumours. Ann. Oncol. 24:84–90.
15. Honda, K., T. Yamada, M. Seike, Y. Hayashida, M. Idogawa, T. Kondo, et al. 2004. Alternative splice variant of actinin-4 in small cell lung cancer. Oncogene 23:5257–5262.
16. Santarius, T., J. Shipley, D. Brewer, M. R. Stratton, and C. S. Cooper. 2010. A census of amplified and overexpressed human cancer genes. Nat. Rev. Cancer 10:59–64.
17. Jouzdani, E., J. Yachouh, V. Costes, J. L. Faillie, C. Cartier, F. Poizat, et al. 2010. Prognostic value of a three-grade classification in primary epithelial parotid carcinoma: result of a histological review from a 20-year experience of total parotidectomy with neck dissection in a single institution. Eur. J. Cancer 46:323–331.
18. Ohtomo, R., T. Mori, S. Shibata, K. Tsuta, A. M. Maeshima, C. Akazawa, et al. 2013. SOX10 is a novel marker of acinus and intercalated duct differentiation in salivary gland tumors: a clue to the histogenesis for tumor diagnosis. Mod. Pathol. 26:1041–1050.
19. Cappuzzo, F., C. Ligorio, L. Toschi, E. Rossi, R. Trisolini, D. Paioli, et al. 2007. EGFR and HER2 gene copy number and response to first-line chemotherapy in patients with advanced non-small cell lung cancer (NSCLC). J. Thorac. Oncol. 2:423–429.
20. Ettl, T., M. Gosau, G. Brockhoff, S. Schwarz-Furlan, A. Agaimy, T. E. Reichert, et al. 2013. Predictors of cervical lymph node metastasis in salivary gland cancer. Head Neck. doi: 10.1002/hed.23332.
21. Seethala, R. R. 2011. Histologic grading and prognostic biomarkers in salivary gland carcinomas. Adv. Anat. Pathol. 18:29–45.
22. Cheuk, W., and J. K. Chan. 2007. Advances in salivary gland pathology. Histopathology 51:1–20.
23. Seethala, R. R., K. Cieply, E. L. Barnes, and S. Dacic. 2011. Progressive genetic alterations of adenoid cystic carcinoma with high-grade transformation. Arch. Pathol. Lab. Med. 135:123–130.
24. Seethala, R. R. 2009. An update on grading of salivary gland carcinomas. Head Neck Pathol. 3:69–77.
25. Ettl, T., S. Schwarz, N. Kleinsasser, A. Hartmann, T. E. Reichert, and O. Driemel. 2008. Overexpression of EGFR and absence of C-KIT expression correlate with poor prognosis in salivary gland carcinomas. Histopathology 53:567–577.
26. Ettl, T., C. Stiegler, K. Zeitler, A. Agaimy, J. Zenk, T. E. Reichert, et al. 2012. EGFR, HER2, survivin, and loss of pSTAT3 characterize high-grade malignancy in salivary gland cancer with impact on prognosis. Hum. Pathol. 43:921–931.
27. Ach, T., K. Zeitler, S. Schwarz-Furlan, K. Baader, A. Agaimy, C. Rohrmeier, et al. 2013. Aberrations of MET are associated with copy number gain of EGFR and loss of PTEN and predict poor outcome in patients with salivary gland cancer. Virchows Arch. 462:65–72.
28. Tonon, G., S. Modi, L. Wu, A. Kubo, A. B. Coxon, T. Komiya, et al. 2003. t(11;19)(q21;p13) translocation in mucoepidermoid carcinoma creates a novel fusion product that disrupts a Notch signaling pathway. Nat. Genet. 33:208–213.
29. West, R. B., C. Kong, N. Clarke, T. Gilks, J. S. Lipsick, H. Cao, et al. 2011. MYB expression and translocation in adenoid cystic carcinomas and other salivary gland tumors with clinicopathologic correlation. Am. J. Surg. Pathol. 35:92–99.
30. Milano, A., F. Longo, M. Basile, R. V. Iaffaioli, and F. Caponigro. 2007. Recent advances in the treatment of salivary gland cancers: emphasis on molecular targeted therapy. Oral Oncol. 43:729–734.
31. Haddad, R., A. D. Colevas, J. F. Krane, D. Cooper, B. Glisson, P. C. Amrein, et al. 2003. Herceptin in patients with advanced or metastatic salivary gland carcinomas. A phase II study. Oral Oncol. 39:724–727.

IJC
International Journal of Cancer

Multilayer-omics analysis of renal cell carcinoma, including the whole exome, methylome and transcriptome

Eri Arai[1]*, Hiromi Sakamoto[2]*, Hitoshi Ichikawa[2], Hirohiko Totsuka[3], Suenori Chiku[4], Masahiro Gotoh[1], Taisuke Mori[1], Tamao Nakatani[1], Sumiko Ohnami[2], Tohru Nakagawa[5], Hiroyuki Fujimoto[5], Linghua Wang[6], Hiroyuki Aburatani[6], Teruhiko Yoshida[2] and Yae Kanai[1]

[1] Division of Molecular Pathology, National Cancer Center Research Institute, Tokyo, Japan
[2] Division of Genetics, National Cancer Center Research Institute, Tokyo, Japan
[3] Bioinfomatics Group, Research and Development Center, Solution Division 4, Hitachi Government and Public Corporation System Engineering Ltd, Tokyo, Japan
[4] Science Solutions Division, Mizuho Information and Research Institute Inc., Tokyo, Japan
[5] Department of Urology, National Cancer Center Hospital, Tokyo, Japan
[6] Genome Science Division, Research Center for Advanced Science and Technology (RCAST), The University of Tokyo, Japan

The aim of this study was to identify pathways that have a significant impact during renal carcinogenesis. Sixty-seven paired samples of both noncancerous renal cortex tissue and cancerous tissue from patients with clear cell renal cell carcinomas (RCCs) were subjected to whole-exome, methylome and transcriptome analyses using Agilent SureSelect All Exon capture followed by sequencing on an Illumina HiSeq 2000 platform, Illumina Infinium HumanMethylation27 BeadArray and Agilent SurePrint Human Gene Expression microarray, respectively. Sanger sequencing and quantitative reverse transcription-PCR were performed for technical verification. MetaCore software was used for pathway analysis. Somatic nonsynonymous single-nucleotide mutations, insertions/deletions and intragenic breaks of 2,153, 359 and 8 genes were detected, respectively. Mutations of *GCN1L1*, *MED12* and *CCNC*, which are members of *CDK8* mediator complex directly regulating β-catenin-driven transcription, were identified in 16% of the RCCs. Mutations of *MACF1*, which functions in the Wnt/β-catenin signaling pathway, were identified in 4% of the RCCs. A combination of methylome and transcriptome analyses further highlighted the significant role of the Wnt/β-catenin signaling pathway in renal carcinogenesis. Genetic aberrations and reduced expression of *ERC2* and *ABCA13* were frequent in RCCs, and *MTOR* mutations were identified as one of the major disrupters of cell signaling during renal carcinogenesis. Our results confirm that multilayer-omics analysis can be a powerful tool for revealing pathways that play a significant role in carcinogenesis.

Cancer Genetics

Key words: *CDK8* mediator complex, clear cell renal cell carcinoma (RCC), multilayer-omics analysis, whole exome analysis, Wnt/β-catenin signaling pathway

Abbreviations: ASCAT: allele-specific copy number analysis of tumors; GeMDBJ: genome medicine database of Japan; GPHMM: global parameter hidden Markov model; indel: insertion/deletion; mTOR: mammalian target of rapamycin; N: non-cancerous renal cortex tissue; PolyPhen: polymorphism phenotyping; RCC: renal cell carcinoma; SIFT: sorting intolerant from tolerant; SNP: single nucleotide polymorphism; T: cancerous tissue

Additional Supporting Information may be found in the online version of this article.

*E.A. and H.S. contributed equally to this work

Grant sponsor: Program for Promotion of Fundamental Studies in Health Sciences (10-41, 10-42 and 10-43), National Institute of Biomedical Innovation (NiBio), Japan; **Grant sponsor:** National Cancer Center Biobank, National Cancer Center Research and Development Fund (23A-1), Japan

DOI: 10.1002/ijc.28768

History: Received 24 July 2013; Accepted 16 Jan 2014; Online 6 Feb 2014

Correspondence to: Yae Kanai, MD, PhD, Division of Molecular Pathology, National Cancer Center Research Institute, 5-1-1 Tsukiji, Chuo-ku, Tokyo 104-0045, Japan, Tel.: +81335422511, Fax: +81-3-3248-2463, E-mail: ykanai@ncc.go.jp or Teruhiko Yoshida, MD, PhD, Division of Genetics, National Cancer Center Research Institute, 5-1-1 Tsukiji, Chuo-ku, Tokyo 104-0045, Japan, Tel.: +81335422511, Fax: +81-3-3541-2685, E-mail: tyoshida@ncc.go.jp

What's new?

Large-scale systems biology approaches are currently reshaping biomedical research identifying new pathways or reinforcing significance of previously discovered pathways in cancer biology. Here the authors performed multilayer -omics analyses in clear renal carcinoma or healthy control samples. They found frequent tumor-associated genetic aberrations of *GCN1L1*, *MED12*, and *CCNC*, all members of the *CDK8* Mediator complex involved in regulating β-catenin-driven transcription, as well as alterations in *MACF1*, also a member of the Wnt/β-catenin signaling pathway. These findings underscore the significance of the Wnt/β-catenin signaling pathway during renal carcinogenesis and confirm the power of large-scale sequencing efforts in revealing pathways that may become therapeutic targets in specific cancers.

Clear cell renal cell carcinoma (RCC) is the most common histological subtype of adult kidney cancer and frequently affects working-age adults in midlife.[1] Recently, large-scale PCR-based exon resequencing and whole-exome analysis by exon capturing have revealed that renal carcinogenesis involves inactivation of histone-modifying genes such as *SETD2*,[2] a histone H3 lysine 36 methyltransferase, *KDM5C*,[2] a histone H3 lysine 4 demethylase and *UTX*,[3] a histone H3 lysine 27 demethylase, as well as the SWI/SNF chromatin remodeling complex gene, *PBRM1*.[4] Moreover, it is well known that clear cell RCCs are characterized by inactivation of the *VHL* tumor-suppressor gene encoding a component of the protein complex that possesses ubiquitin ligase E3 activity.[5] Another exome analysis study has revealed frequent mutation of a further component of the ubiquitin-mediated proteolysis pathway, *BAP1*.[6] Non-synonymous mutations of the *NF2* gene and truncating mutations of the *MLL2* gene have also been reported.[2]

Not only genetic, but also epigenetic events appear to accumulate during carcinogenesis, and DNA methylation alterations are one of the most consistent epigenetic changes in human cancers.[7,8] In fact, we have shown that noncancerous renal tissue obtained from patients with RCCs is already at the precancerous stage associated with DNA methylation alterations, even though no remarkable histological changes are evident and there is no association with chronic inflammation or persistent infection with viruses or other pathogens.[9,10] Furthermore, using single-CpG resolution methylome analysis with the Infinium array, we have demonstrated that DNA methylation alterations at precancerous stages may determine tumor aggressiveness and patient outcome.[11]

It is well known that DNA methylation alterations around promoter regions affect the expression levels of tumor-related genes.[7] Once the DNA methylation status has been altered, such alterations are stably preserved on the DNA double strands by covalent bonds through maintenance-methylation mechanisms by *DNMT1* during carcinogenesis.[7] Therefore, tumor-related genes showing alterations of both expression level and DNA methylation may have a larger impact on carcinogenesis than those showing only alterations of expression. Therefore, subjecting tissue specimens to a combination of both methylome and transcriptome analyses may be a powerful approach for revealing genes that are involved in carcinogenetic pathways.

Although one article reporting the use of an integrated multilayer-omics approach including exome analysis to examine human clear cell RCCs was published while this manuscript was in preparation,[12] the entire pathway of carcinogenesis in the kidney may not yet be fully explained. In this study, to identify pathways having a significant impact during renal carcinogenesis, we subjected paired samples of both noncancerous renal cortex tissue (N) and cancerous tissue (T) from patients with clear cell RCCs to whole-exome, methylome and transcriptome analyses.

Material and Methods

Patients and tissue samples

Sixty-seven paired T and N samples were obtained from materials that had been surgically resected from 67 patients with primary clear cell RCCs. N mainly consists of proximal tubules, which are the origin of clear cell RCCs. These patients had not received any preoperative treatment and had undergone nephrectomy at the National Cancer Center Hospital, Tokyo. Tissue specimens were provided by the National Cancer Center Biobank, Tokyo. Histological diagnosis was made in accordance with the World Health Organization classification.[13] All the tumors were graded on the basis of previously described criteria[14] and classified according to the pathological Tumor-Node-Metastasis classification.[15] The clinicopathological parameters of these RCCs are summarized in Supporting Information Table S1.

All patients included in this study provided written informed consent. This study was approved by the Ethics Committee of the National Cancer Center, Tokyo and was performed in accordance with the Declaration of Helsinki.

Exome analysis

High-molecular-weight DNA was extracted using phenol-chloroform, followed by dialysis. Three-microgram aliquots of genomic DNA from the 67 paired samples were fragmented by a Covaris-S2 instrument (Covaris, Woburn, MA) to provide DNA fragments with a base pair peak at 150–200 bp. The DNA fragments were end-repaired and ligated with paired-end adaptors (NEBNext DNA sample prep, New England Biolabs, Ipswich, MA). The resulting DNA library was purified using Agencourt AMPure XP Reagent (Beckman Coulter Genomics, Danvers, MA) and amplified by PCR (4 cycles). Five-hundred-nanogram aliquots of the adaptor-ligated libraries were

Table 1. Genes showing 3 or more genetic aberration scores in clear cell RCCs

			Genetic aberration score				Predicted protein function				
							Nonsynonymous single-nucleotide mutation[2]		Indel	Copy number aberration (%)[3]	
Genes	Chr[1]	Entrez Gene ID	Non-synonymous single-nucleotide mutation	Indel	Intragenic break	Total	SIFT	PolyPhen-2	SIFT	Loss	Gain
VHL	3	7,428	22	14	0	36	0	1	Damaging	77.61	11.94
PBRM1	3	55,193	11	10	1	22	0	1	Damaging	73.13	10.45
TTN	2	7,273	9	3	0	12	0.75	0.387878	Neutral	0.00	38.81
KDM5C	X	8,242	4	4	0	8	0	0.998	Damaging	53.73	26.87
MUC16	19	94,025	6	0	0	6	0	NA	–	2.99	29.85
CUBN	10	8,029	5	1	0	6	0.32	0.987	Damaging	0.00	26.87
SETD2	3	29,072	3	3	0	6	0	0.99	Damaging	76.12	7.46
ABCA13	7	154,664	5	0	0	5	0	NA	–	0.00	44.78
BIRC6	2	57,448	4	1	0	5	0.02	NA	Damaging	4.48	35.82
GCN1L1	12	10,985	3	2	0	5	0	0.735079	Damaging	0.00	37.31
HERC2	15	8,924	5	0	0	5	0.01	0.902	–	1.49	25.37
BAP1	3	8,314	4	0	0	4	0	1	–	74.63	10.45
KIAA0100	17	9,703	4	0	0	4	0.05	0.999	–	0.00	29.85
MTOR	1	2,475	4	0	0	4	0	0.999	–	7.46	25.37
SPTBN1	2	6,711	3	1	0	4	0	0.993	NA	0.00	35.82
SPTA1	1	6,708	2	2	0	4	0.09	0.513	Damaging	0.00	34.33
CADM2	3	253,559	1	0	3	4	0.09	0.012	–	29.85	25.37
ERC2	3	26,059	1	0	3	4	0.01	NA	–	71.64	10.45
ADAM23	2	8,745	3	0	0	3	0	0.998	–	2.99	37.31
AKAP9	7	10,142	3	0	0	3	0	0.986	–	0.00	46.27
ANKRD26	10	22,852	3	0	0	3	0	0.995	–	2.99	28.36
ARHGEF33	2	100,271,715	3	0	0	3	0	NA	–	2.99	35.82
BRD4	19	23,476	3	0	0	3	0	0.997	–	0.00	29.85
C1orf112	1	55,732	3	0	0	3	0	0.952	–	0.00	34.33
CCNC	6	892	3	0	0	3	0	0.876	–	2.99	22.39
CPAMD8	19	27,151	3	0	0	3	0	0.439286	–	0.00	29.85
CSMD3	8	114,788	3	0	0	3	0	0.999	–	1.49	31.34
DNAH5	5	1,767	3	0	0	3	0.1	0.169	–	0.00	46.27
FAT1	4	2,195	3	0	0	3	0	NA	–	1.49	22.39
FAT2	5	2,196	3	0	0	3	0	0.999	–	0.00	71.64
FMN2	1	56,776	3	0	0	3	0	0.957	–	0.00	34.33
FNIP1	5	96,459	3	0	0	3	0.1	0.45171	–	0.00	65.67
KIF26B	1	55,083	3	0	0	3	0	NA	–	0.00	34.33
LIMCH1	4	22,998	3	0	0	3	0	0.992	–	2.99	20.90
LRBA	4	987	3	0	0	3	0.01	0.939	–	1.49	23.88
MACF1	1	23,499	3	0	0	3	0	0.791225	–	4.48	25.37
MADD	11	8,567	3	0	0	3	0	0.999	–	0.00	29.85
MED12	X	9,968	3	0	0	3	0.01	0.576	–	55.22	25.37
MGAM	7	8,972	3	0	0	3	0	NA	–	0.00	46.27
OBSCN	1	84,033	2	1	0	3	0	NA	Neutral	1.49	34.33

Table 1. Genes showing 3 or more genetic aberration scores in clear cell RCCs (Continued)

			Genetic aberration score				Predicted protein function: Nonsynonymous single-nucleotide mutation[2]		Predicted protein function: Indel	Copy number aberration (%)[3]	
Genes	Chr[1]	Entrez Gene ID	Non-synonymous single-nucleotide mutation	Indel	Intragenic break	Total	SIFT	PolyPhen-2	SIFT	Loss	Gain
PLCE1	10	51,196	3	0	0	3	0	0.999	–	10.45	25.37
PREX2	8	80,243	3	0	0	3	0	1	–	5.97	31.34
PTPN4	2	5,775	3	0	0	3	0	0.999	–	0.00	35.82
ROR2	9	4,920	3	0	0	3	0	1	–	7.46	20.90
RP1	8	6,101	3	0	0	3	0.01	0.992	–	5.97	31.34
RYR2	1	6,262	3	0	0	3	0	NA	–	0.00	34.33
SYNE1	6	23,345	3	0	0	3	0.04	0.918	–	4.48	20.90
TTI1	20	9,675	3	0	0	3	0	0.999	–	0.00	29.85
VWDE	7	221,806	3	0	0	3	0.04	NA	–	0.00	44.78
ATM	11	472	2	1	0	3	0	1	NA	7.46	28.36
DNAH2	17	146,754	2	1	0	3	0.14	0.048	Damaging	0.00	29.85
FOXN2	2	3,344	2	1	0	3	0.08	0.255	Neutral	1.49	35.82
PTEN	10	5,728	2	1	0	3	0.01	0.988	Damaging	8.96	25.37
SAMD9L	7	219,285	2	1	0	3	0	0.968	Damaging	0.00	46.27
SI	3	6,476	2	1	0	3	0.01	0.992	Damaging	10.45	32.84
TCHH	1	7,062	2	1	0	3	NA	0.998	Damaging	0.00	34.33
TUBGCP6	22	610,053	2	1	0	3	0	0.993	NA	1.49	29.85
UGGT2	13	55,757	2	1	0	3	0.01	0.726	Neutral	0.00	25.37
CCDC178	18	374,864	1	2	0	3	0	0.235	Damaging	2.99	22.39
HGSNAT	8	138,050	1	2	0	3	0	NA	Damaging	16.42	25.37
NIPBL	5	25,836	1	2	0	3	0.05	0.98	Damaging	0.00	46.27

[1]Chromosome.
[2]Minimum SIFT score and maximum PolyPhen-2 score among all detected mutations of each gene (A SIFT score of <0.05 means "damaging."[19] PolyPhen-2 scores of >0.85 and 0.15–0.85 mean "probably damaging" and "possibly damaging," respectively).[20] NA: not available using SIFT or PolyPhen-2; –: indels of the gene were not detected.
[3]The incidence of loss (1 or less copy number) or gain (3 or more copy number) detected using ASCAT or GPHMM in all 67 tumors. SIFT and PolyPhen-2 scores and copy numbers of each gene in each RCC were described in Supporting Information Table S3.

hybridized for 24 hr at 65°C with biotinylated oligo RNA bait, SureSelect Human All Exon 50 Mb (Agilent Technologies, Santa Clara, CA). The hybridized genomic DNA was subjected to 10 cycles of PCR reamplification. Following the manufacturer's standard protocols, the whole-exome DNA library was sequenced on an Illumina HiSeq 2000 (Illumina, San Diego, CA) using 75-bp paired-end reads.

After completion of the entire run, image analyses, error estimation and base calling were performed using the Illumina Pipeline (version 1.3.4) to generate primary data. First, the reads were aligned against the reference human genome from UCSC human genome 19 (Hg19) using the Burrows Wheeler Aligner Multi-Vision software package.[16] Because duplicated reads had been generated during the PCR amplification process, paired-end reads that were aligned to the same genomic positions were removed using SAMtools. Second, the following loci were removed: (*i*) read depth <6 and (*ii*) base quality score <3 in the T sample. Third, we used the following Bayesian data analysis pipeline developed in our laboratory: (*i*) single nucleotide polymorphism (SNP) array analysis was performed on each paired cancerous and noncancerous tissue samples using Illumina HumanOmni1-Quad BeadChip (see "SNP microarray analysis") and the genomic region, which is considered to be 1 copy in the pure cancerous genome was identified by the visual inspection of the log R ratio and B allele frequency plots on the Illumina Genome Viewer in the GenomeStudio software. (*ii*) Heterozygous SNP loci were selected from the above 1-copy region using GATK UnifiedGenotyper (Broad Institute, MA). (*iii*) At the SNP loci, which were 1 copy in the pure cancerous genome but heterozygous in the noncancerous genome, the ratio of the contaminating non-cancerous cells in the

cancerous tissue was estimated from the allele frequencies of the cancerous genome by fitting to a binominal mixture model. (*iv*) Considering the estimated ratio of the contaminating noncancerous cells, the posterior probability of the genotypes of the cancer cells was calculated. Mutation was called if the posterior probability of being homozygous for the allele recorded in the reference human genome sequence was 0.001 or lower, and the ratio of the nonreference allele was 0.02 or lower in the noncancerous tissue sample, which had a read depth of at least 15. Fourth, Annovar extracted candidates that were nonsynonymous and did not correspond to the refSNP number. Fifth, candidates were discarded if the frequency of the nonreference allele was >2% in the N sample. Somatic mutations were also removed from the candidates if the root mean square mapping quality score of the reads covering the somatic mutation was <20. Finally, if the Blast search did not detect homologous regions for which the edit distance was 7 or <7 within the neighboring 151-bp stretch (75 bp both up- and downstream), the candidate was considered as a somatic mutation. Somatic insertions/deletions (indels) were called using both SAMtools and Pindel[17] as described previously.[18] Effects of amino acid substitutions on protein function due to single nucleotide nonsynonymous mutations have been estimated using the Sorting Intolerant from Tolerant (SIFT) (http://sift.jcvi.org)[19] and polymorphism phenotyping (PolyPhen)-2 (http://genetics.bwh.harvard.edu/pph2/),[20] and those due to indels have been estimated using SIFT.[21] All data from exome analysis will be submitted to the Genome Medicine Database of Japan (GeMDBJ, https://gemdbj.nibio.go.jp/dgdb/).

Sanger sequencing

To verify the nonsynonymous single-nucleotide mutations and indels detected by the exome analysis and described in Table 1, the target sites and the flanking sequences of each patient's DNA template were amplified individually with specific primers designed using Primer6.0. The PCR products were then sequenced with an ABI 3730 DNA Analyzer using the BigDye Terminator v1.1 Cycle Sequencing kit (Life Technologies, Carlsbad, CA).

SNP microarray analysis

Two-hundred-nanogram aliquots of DNA from the 67 paired samples were genotyped with the HumanOmni1-Quad BeadChip (Illumina) in accordance with the manufacturer's protocols. The data were assembled using GenomeStudio software (Illumina). For the single-nucleotide mutation detection, we developed the Bayesian data analysis pipeline using SNP microarray data (see "Exome analysis"). Localization of intragenic breakpoints, in which the end point of a deletion or duplication lies within a gene, in each of the T samples was clearly identified by the visual inspection of the B allele frequency plots on the Illumina Genome Viewer in the GenomeStudio software (Supporting Information Fig. S1). Copy number data has been obtained using Allele-Specific Copy Number Analysis of Tumors (ASCAT; http://heim.ifi.uio.no/bioinf/Projects/ASCAT/)[22] and Global Parameter Hidden Markov Model (GPHMM; http://bioinformatics.ustc.edu.cn/gphmm/)[23] software.

Infinium analysis

Five-hundred-nanogram aliquots of DNA from the 67 paired samples were subjected to bisulfite conversion using an EZ DNA Methylation-Gold™ Kit (Zymo Research, Irvine, CA). Subsequently the DNA methylation status at 27,578 CpG loci was examined at single-CpG resolution using the Infinium HumanMethylation27 Bead Array (Illumina). The data were assembled using GenomeStudio methylation software (Illumina). At each CpG site, the ratio of the fluorescent signal was measured using a methylated probe relative to the sum of the methylated and unmethylated probes, that is, the so-called β-value, which ranges from 0.00 to 1.00, reflecting the methylation level of an individual CpG site. All data of Infinium analysis will be submitted to GeMDBJ.

Pyrosequencing

DNA methylation levels of Infinium probe sites of the *RAB25, GGT6, C3* and *CHI3L2* genes and the 5′-region of the *ABCA13* gene were measured by pyrosequencing. The PCR and sequencing primers were designed using Pyrosequencing Assay Design Software ver.1.0 (QIAGEN, Hilden, Germany). To overcome any PCR bias, we optimized the annealing temperature as described previously.[24] Each of the primer sequences and PCR conditions are given in Supporting Information Figure S2. The PCR product was generated from bisulfite-treated DNA and subsequently captured on streptavidin-coated beads. Quantitative sequencing was performed on a PyroMark Q24 (QIAGEN) using the Pyro Gold Reagents (QIAGEN) in accordance with the manufacturer's protocol.

Expression microarray analysis

Total RNA was isolated using TRIzol reagent (Life Technologies). From the 67 paired samples, 29 pairs, from which a sufficient amount of total RNA for both N and T samples was available, were subjected to expression microarray analysis. Two-hundred-nanogram aliquots of total RNA from the 29 paired samples were used for the production of fluorescent complementary RNA, and all samples were hybridized to the SurePrint G3 Human Gene Expression 8 × 60 K microarray (Agilent Technologies). The signal values were extracted using the Feature Extraction software (Agilent Technologies). All data of Expression microarray analysis will be submitted to GeMDBJ.

Quantitative RT-PCR analysis

cDNA was reverse-transcribed from total RNA using random primers and Superscript III RNase H$^-$ Reverse Transcriptase (Life Technologies). From the 67 paired samples, 66 pairs, from which a sufficient amount of cDNA for both N and T

samples was available, were subjected to quantitative RT-PCR analysis. mRNA expression was analyzed using custom TaqMan Expression Assays (probe and PCR primer sets, Supporting Information Table S2) on the 7500 Fast Real-Time PCR System employing the relative standard curve method. All CT values were normalized to that of *GAPDH* in the same sample.

Multilayer-omics scoring

If any of the somatic nonsynonymous single-nucleotide mutations, indels or intragenic breaks was observed in one of the T samples, a genetic aberration score of one was assigned for the gene. If the $\Delta\beta$ ($\beta_T - \beta_N$) was 0.2 or more, the gene was considered to be hypermethylated in the T sample relative to the corresponding N sample. If the $\Delta\beta$ ($\beta_T - \beta_N$) was -0.2 or less, the gene was considered to be hypomethylated in the T sample relative to the corresponding N sample.

The expression level (E value) of each gene was expressed as the log2-signal intensity normalized by the median for all probes in the sample. If the ΔE ($E_T - E_N$) was 4 or more, the expression of the gene was considered to be elevated in the T sample relative to the corresponding N sample. If the ΔE ($E_T - E_N$) was -4 or less, the expression of the gene was considered to be reduced in the T sample relative to the corresponding N sample.

All probes of the Infinium HumanMethylation27 Bead Array and SurePrint G3 Human Gene Expression 8 × 60 K microarray were aligned against the reference human genome from Hg19. Infinium array probe and expression microarray probe pairs were annotated to each individual gene. If the probe of the Infinium array was designed for the upstream region including the promoter region, exon 1 or intron 1 of the gene, if $\Delta\beta$ ($\beta_T - \beta_N$) of the gene was 0.2 or more (DNA hypermethylation), and if ΔE ($E_T - E_N$) based on the expression microarray was -4 or less (reduced expression) in one paired sample of T and N, then a gene downregulation score of one was assigned. If the probe of the Infinium array was designed for the upstream region including the promoter region, exon 1 or intron 1 of the gene, if $\Delta\beta$ of the gene was -0.2 or less (DNA hypomethylation), and if ΔE ($E_T - E_N$) based on the expression microarray was 4 or more (overexpression) in one paired sample of T and N, then a gene upregulation score of one was assigned.

Pathway analysis

MetaCore software (http://www.genego.com) is a pathway analysis tool based on a proprietary manually curated database of human protein–protein, protein–DNA and protein compound interactions. The MetaCore pathway analysis by GeneGo was performed among genes showing genetic scores of 3 or more or showing downregulation or upregulation scores of 5 or more. Pathways for which the p value was <0.05 were considered to play a significant role in renal carcinogenesis.

Results

Genetic aberrations

Exome analysis detected somatic non-synonymous single-nucleotide mutations and indels of 2,153 and 359 genes among the 67 clear cell RCCs, respectively. SNP array analysis revealed intragenic breaks in 8 genes among the 67 RCC samples. In total, 2,440 genes showed non-synonymous single-nucleotide mutations, indels and/or intragenic breaks in RCCs and were assigned genetic aberration scores (described in "Multilayer-omics scoring" in the Material and Methods section) of 1 or more. Genetic alterations in each RCC are summarized in Supporting Information Table S3. The 2,131 and 248 genes that were assigned a genetic aberration score of 1 and 2 are listed in Supporting Information Table S4, and the 61 genes that were assigned genetic aberration scores of 3 or more are listed in Table 1. All 256 mutations (209 somatic nonsynonymous single-nucleotide mutations and 57 indels with 10 exceptions, for which Sanger sequencing failed due to difficulties with PCR primer design) listed in Table 1 were verified by Sanger sequencing. In addition, mutations of 54 (89%) of the 61 genes included in Table 1 were also found in the clear cell RCC database in The Cancer Genome Atlas (http://cancergenome.nih.gov/; Supporting Information Table S5), indicating the reliability of our whole-exome analysis results.

Effects of amino acid substitutions due to genetic aberrations on protein function estimated using SIFT[19,21] and PolyPhen-2[20] software are shown in Table 1 and Supporting Information Table S3. In 60 of 61 genes listed in Table 1, SIFT and PolyPhen-2 analyses (less than 0.05 SIFT score[19] or more than 0.15 PolyPhen-2 score[20] for nonsynonymous single-nucleotide mutations and "damaging" SIFT score[21] for indels) indicated that amino acid substitutions due to genetic aberrations impair the functions of proteins.

The incidence of copy number loss (1 or less) and gain (3 or more), detected using ASCAT[22] and GPHMM[23] software, of the genes that were assigned genetic aberration scores of 3 or more is described in Table 1. The copy number of each gene showing genetic aberrations in each RCC is described in Supporting Information Table S3. Nonsynonymous single-nucleotide mutations and indels were frequently concordant with copy number alterations (Table 1), suggesting that such genetic aberrations may actually result in dysfunction of proteins in RCCs.

In addition to recurrent genetic aberrations, expression microarray analysis revealed reduced mRNA expression [ΔE ($E_T - E_N$) was -4 or less as described in "Expression microarray analysis" in the Material and Methods section] of the *ERC2* and *ABCA13* genes in 21 and 31% of RCCs, respectively. These mRNA expression alterations were verified quantitatively by real-time RT-PCR analysis [mean *ERC2* expression levels in T samples ($n = 66$): 8.91 ± 29.72; those in N samples ($n = 66$): 110.02 ± 75.31 ($p < 1.00 \times 10^{-12}$, Mann-Whitney U-test) and mean *ABCA13* expression levels in T samples ($n = 66$): 8.43 ± 45.12; those in N samples ($n = 66$): 47.82 ± 89.51 ($p < 1.00 \times 10^{-12}$, Mann-Whitney U-test)].

Probes for the *ERC2* gene were designed for the Infinium array, and DNA hypermethylation around the 5′-region of the *ERC2* gene was detected in only 6% of RCCs, indicating that reduced expression of the *ERC2* gene may not be attributable to DNA methylation alterations during renal carcinogenesis. Since the probes for the *ABCA13* gene were not designed for the Infinium array, we examined DNA methylation levels in the 5′-region of the *ABCA13* gene by pyrosequencing. No significant differences in the DNA methylation levels of the *ABCA13* gene between T samples (0.528 ± 0.060, $n = 67$) and N samples (0.510 ± 0.149, $n = 67$) were observed (Supporting Information Fig. S2a). Our data for RCCs were consistent with the data in the public database Gene Expression Omnibus (http://www.ncbi.nlm.nih.gov/geo/): no significant differences in DNA methylation levels of the *ABCA13* gene were evident between bile duct cancer and normal bile duct tissue (Accession number: GSE49656) and between breast cancer and normal breast tissue (GSE37754), indicating that reduced expression of the *ABCA13* gene may not be attributable to DNA methylation alterations during renal carcinogenesis.

Alterations of expression associated with DNA hypermethylation or hypomethylation

All genes showing DNA methylation alterations [0.2 or more $\Delta\beta$ ($\beta_T - \beta_N$) or -0.2 or less $\Delta\beta$ ($\beta_T - \beta_N$)] or mRNA expression alterations [4 or more ΔE ($E_T - E_N$) or -4 or less ΔE ($E_T - E_N$)] in each RCC are summarized in Supporting Information Table S6 along with genes showing genetic aberration scores of 1 or more. The DNA methylation status of the 5′-region can regulate the mRNA expression level of each gene. DNA methylation status is stably preserved on DNA double strands by covalent bonds and inherited through cell division by maintenance-methylation mechanisms by *DNMT1*. Therefore, altered mRNA expression due to DNA methylation alterations may be more stably fixed during multistage human carcinogenesis in comparison to mRNA expression alterations without DNA methylation alterations. Therefore, we have calculated upregulation and downregulation scores based on both DNA methylation status and expression levels described in the Material and Methods section: 86 genes showed reduced expression [-4 or less ΔE ($E_T - E_N$)] associated with DNA hypermethylation [0.2 or more $\Delta\beta$ ($\beta_T - \beta_N$)] in 5 or more patients (downregulation scores of 5 or more; Table 2) and 28 genes showed overexpression [4 or more ΔE ($E_T - E_N$)] associated with DNA hypomethylation [-0.2 or less $\Delta\beta$ ($\beta_T - \beta_N$)] in 5 or more patients (upregulation scores of 5 or more; Table 2).

Expression alterations of genes included in Table 2 were validated using the clear cell RCC database in the Gene Expression Omnibus (http://www.ncbi.nlm.nih.gov/geo/; Supporting Information Table S7): reduced or increased mRNA expression of 97 (89%) of the109 genes, which are included in Table 2 and for which probes were designed in the expression microarrays described in the database, were found, indicating the reliability of our expression analysis. Since genome-wide DNA methylation data for RCCs obtained using array-based analysis with appropriate resolution were not available in the public database, Infinium assay data for other human malignant tumors deposited in the Gene Expression Omnibus database (http://www.ncbi.nlm.nih.gov/geo/) were used instead for validation (Supporting Information Table S8). In addition, DNA methylation levels of the representative genes, *RAB25*, *GGT6*, *C3* and *CHI3L2*, included in Table 2 based on the Infinium assay were successfully verified using pyrosequencing (Supporting Information Figs. S2*b*–S2*e*), indicating the reliability of our Infinium assay.

Pathway analysis

MetaCore pathway analysis by GeneGo was performed for 61 genes assigned genetic aberration scores of 3 or more, 86 genes assigned downregulation scores of 5 or more (frequent reduction of expression associated with DNA hypermethylation) and 28 genes assigned upregulation scores of 5 or more (frequent overexpression associated with DNA hypomethylation; total 174 genes). Twenty potentially significant GeneGo pathways ($p < 0.05$) and the affected genes are listed in Table 3. Mutations of 5 (100%) of the 5 genes included in Table 3 were found in the clear cell RCC database of The Cancer Genome Atlas (Supporting Information Table S5). Reduced or increased mRNA expression of 11 (92%) of the 12 genes, which are included in Table 3 and for which probes had been designed in expression microarrays described in the clear cell RCC database of the Gene Expression Omnibus, were found (Supporting Information Table S7), supporting the participation of these genes in renal carcinogenesis.

Genes for which correlation with Wnt/β-catenin signaling was indicated by MetaCore pathway analysis, together with their genetic aberration, DNA methylation alterations and mRNA expression alterations, are illustrated schematically in Figure 1. Mutations, mRNA expression alterations or DNA methylation alterations of 32 (89%) of the 36 genes included in Figure 1 were found in Supporting Information Tables S5, S7 or S8, supporting the participation of the Wnt/β-catenin signaling pathway in renal carcinogenesis. In addition, MetaCore pathway analysis was separately performed for RCCs with and without genetic aberrations and/or DNA hypermethylation [$\Delta\beta$ ($\beta_T - \beta_N$) >0.2] of the *VHL* gene (Supporting Information Table S9 and Fig. S3).

Discussion

High frequencies of genetic aberrations of the *VHL* (53%), *PBRM1* (33%), *KDM5C* (12%) and *SETD2* (9%) genes, which have been highlighted in previous resequencing[2] and exome analyses,[4,6] supported the reliability of our approach. In addition to *PBRM1*, somatic mutation of another member of the SWI/SNF complex, *SMARCA4*, was detected. In addition to *SETD2* and *KDM5C*, somatic mutation of another histone modification protein, *JARID2*, was also detected. The significance of aberrations of chromatin remodeling and histone modification-related proteins in RCCs was confirmed.

Table 2. Genes showing downregulation or upregulation scores of 5 or more in clear cell RCCs

Gene	Chromosome	Entrez GeneID	Downregulation score[1]
(a) Genes showing reduced mRNA expression associated with DNA hypemethylation in their 5′-regions			
CLCNKB	1	1,188	24
SCNN1A	12	6,337	24
RAB25	1	57,111	22
TMEM213	7	155,006	22
ATP6V0A4	7	50,617	22
NR0B2	1	8,431	21
KCNJ1	11	3,758	21
GGT6	17	124,975	21
CLDN8	21	9,073	20
CLDN19	1	149,461	19
MUC15	11	143,662	16
RANBP3L	5	202,151	15
HRG	3	3,273	14
TSPAN8	12	7,103	14
RGS7	1	6,000	11
PTH1R	3	5,745	11
CWH43	4	80,157	11
F11	4	2,160	11
IRX2	5	153,572	11
EHF	11	26,298	11
CBLC	19	23,624	11
ATP6V1B1	2	525	10
LRRC2	3	79,442	10
CLDN16	3	10,686	10
EGF	4	1,950	10
WISP3	6	8,838	10
PHYHD1	9	254,295	10
FLJ45983	10	399,717	10
WIT-AS	11	51,352	10
ACSF2	17	80,221	10
ALDOB	9	229	9
ANKRD2	10	26,287	9
WT1	11	7,490	9
SOST	17	50,964	9
CYP4F3	19	4,051	9
COL18A1-AS1	21	378,832	9
BSND	1	7,809	8
TACSTD2	1	4,070	8
SLC44A4	6	80,736	8
KHDRBS2	6	202,559	8
VWC2	7	375,567	8
CHRM1	11	1,128	8
COL4A6	X	1,288	8
XPNPEP2	X	7,512	8
PROM2	2	150,696	7
ACPP	3	55	7
CKMT2	5	1,160	7
NEFM	8	4,741	7
KCNA4	11	3,739	7
FLRT1	11	23,769	7
OLFM4	13	10,562	7
SERPINA4	14	5,267	7
STRA6	15	64,220	7
CRABP1	15	1,381	7
SLC7A10	19	56,301	7
CSDC2	22	27,254	7
VWA5B1	1	127,731	6
LAD1	1	3,898	6
SYN2	3	6,854	6
SLC22A13	3	9,390	6
ABHD14A	3	25,864	6
UPK1B	3	7,348	6
KCTD8	4	386,617	6
SFRP1	8	6,422	6
GATA3	10	2,625	6
DAO	12	1,610	6
TMPRSS3	21	64,699	6
CHD5	1	26,038	5
PRELP	1	5,549	5
PLD5	1	200,150	5
MAL	2	4,118	5
ENTPD3	3	956	5
TNNC1	3	7,134	5
ANK2	4	287	5
PART1	5	25,859	5
SVOPL	7	136,306	5
DMRT2	9	10,655	5
AMBP	9	259	5
RBP4	10	5,950	5
SLC22A12	11	116,085	5
PDZRN4	12	29,951	5
PROZ	13	8,858	5
RHCG	15	51,458	5
KLK6	19	5,653	5

Table 2. Genes showing downregulation or upregulation scores of 5 or more in clear cell RCCs (Continued)

Gene	Chromosome	Entrez GeneID	Downregulation score[1]
BEX1	X	55,859	5
ZCCHC16	X	340,595	5
Gene	**Chromosome**	**Entrez GeneID**	**Up-regulation score[2]**
(b) Genes showing increased mRNA expression associated with DNA hypomethylation in their 5′-regions.			
CA9	9	768	25
C3	19	718	23
CP	3	1,356	22
NNMT	11	4,837	21
FABP7	6	2,173	11
REG1A	2	5,967	10
UBD	6	10,537	8
ENPP3	6	5,169	8
MCHR1	22	2,847	7
FCGR3A	1	2,214	6
FGG	4	2,266	6
PMCHL1	5	5,369	6
CPA6	8	57,094	6
SAA2	11	6,289	6
SAA1	11	6,288	6
DNAJB13	11	374,407	6
VWF	12	7,450	6
FGF11	17	2,256	6
SPAG4	20	6,676	6
CHI3L2	1	1,117	5
FCRL3	1	115,352	5
TIGIT	3	201,633	5
APOLD1	12	81,575	5
CCL18	17	6,362	5
CARD14	17	79,092	5
LILRA2	19	11,027	5
CXorf36	X	79,742	5
SH2D1A	X	4,068	5

[1]If the probe of the Infinium array was designed in the 5′-region of the gene, if $\Delta\beta$ ($\beta_T - \beta_N$) was 0.2 or more (DNA hypermethylation) and if ΔE ($E_T - E_N$) based on the expression microarray was −4 or less (reduced expression) in one paired sample (T and N), then a gene downregulation score of 1 was assigned.
[2]If the probe of the Infinium array was designed in the 5′-region of the gene, if $\Delta\beta$ ($\beta_T - \beta_N$) was −0.2 or less (DNA hypomethylation) and if ΔE ($E_T - E_N$) based on the expression microarray was 4 or more (overexpression) in one paired sample (T and N), then a gene upregulation score of 1 was assigned.

Among genes showing frequent genetic aberrations (genetic aberration score of 4 or more in Table 1), *GCN1L1* has recently been reported to be associated with the *CDK8* mediator complex, which includes *CDK8*, cyclin C (also known as *CCNC*), *MED12* and *MED13*.[25] *CDK8* directly regulates β-catenin-driven transcription[25] and human *CDK8* is known to be an oncogene that is amplified in a subset of colon cancers.[26] In addition, our quantitative RT-PCR analysis revealed a tendency for down regulation of β-catenin after knockdown of CDK8 by siRNA in RCC cell lines A-498 and ACHN (Supporting Information Fig. S4). These results are consistent with those of previous studies showing that knockdown of CDK8 in the human colon cancer cell line HCT116[27] and the human gastric cancer cell line SNU-638[28] resulted in significant reduction of β-catenin, indicating correlations between *CDK8* and the Wnt/β-catenin pathway.

The fly *MED12* and *MED 13* homologs, kohtalo and skuld, respectively activate Wnt/β-catenin target genes through direct interaction with the Wnt pathway component Pygopus.[29] However, *let-19* and *doy-22*, homologs of human *MED12* and *MED13*, respectively, in *Caenorhabditis elegans*, suppress the transcription of Wnt/β-catenin target genes.[30] Frequent mutation of human *MED12* has been reported in human uterine leiomyomas.[31] Deletion of the *CCNC* gene is frequently detected in human lymphoid malignancies[32] and sarcomas.[33] Wnt/β-catenin signaling is constitutively active in RCCs and activates their cell growth and metastasis.[34] However, unlike other human carcinomas, the incidence of mutation of exon 3 of the β-catenin gene is not so high in RCCs.[34] Analogously with other members of the *CDK8* mediator complex, mutations of *GCN1L1* may participate in renal carcinogenesis *via* Wnt/β-catenin signaling.

All 5 amino acid substitutions of the *GCN1L1* occurred within or near to Huntingtin protein, eEF3, protein phosphatase 2A and TOR (HEAT) repeats, which are crucial for protein-protein interaction[35] (Supporting Information Fig. S5). In addition, SIFT and PolyPhen-2 software predicted that amino acid substitutions due to mutations of the *GCN1L1* gene result in dysfunction of GCN1L1 protein (Table 1). The present study demonstrated not only a genetic aberration score of 5 for *GCN1L1*, but also a genetic aberration score of 3 for *MED12* and *CCNC* (Table 1). SIFT and PolyPhen-2 analyses have predicted that amino acid substitutions due to mutations of the *MED12* and *CCNC* genes also result in dysfunction of the proteins (Table 1). Taken together, the present data indicate that the function of the *CDK8* mediator complex may have been disturbed in 16% of the examined 67 RCCs. Genetic aberrations in members of the *CDK8* mediator complex may thus participate in the Wnt/β-catenin-related carcinogenetic pathway in clear cell RCCs.

MACF 1, a member of the plakin family of cytoskeletal linker proteins, regulates dynamic interactions between actin and microtubules to sustain directional cell movement.[36] *MACF1* is known to function in the Wnt signaling pathway through association with a complex containing axin, β-catenin, *GSK3β* and *APC* during mouse embryogenesis.[36] Somatic mutation of *MACF1* (Table 1) may also participate in the Wnt/β-catenin-related carcinogenetic pathway in clear cell RCCs. With respect

Table 3. Statistically significant GeneGo pathway maps revealed by MetaCore pathway analysis

		Involved genes		
Pathway	*P*-value	Genes	Entrez Gene ID	Multilayer-omics scoring (exome, methylome and transcriptome)
Cell adhesion_tight junctions	9.98×10^{-4}	*CLDN8*	9073	Downregulation score 20
		CLDN16	10686	Downregulation score 10
		CLDN19	149461	Downregulation score 19
Blood coagulation	1.26×10^{-3}	*VWF*	7450	Upregulation score 6
		F11	2160	Downregulation score 11
		FGG	2266	Upregulation score 6
Translation_non-genomic (rapid) action of androgen receptor	1.36×10^{-3}	*MTOR*	2475	Genetic score 4
		PTEN	5728	Genetic score 3
		EGF	1950	Downregulation score 10
Signal transduction_PTEN pathway	2.04×10^{-3}	*MTOR*	2475	Genetic score 4
		PTEN	5728	Genetic score 3
		EGF	1950	Downregulation score 10
Development_EGFR signaling *via* PIP3	7.04×10^{-3}	*PTEN*	5728	Genetic score 3
		EGF	1950	Downregulation score 10
Protein folding and maturation_-Bradykinin/ Kallidin maturation	1.34×10^{-2}	*KLK6*	5653	Downregulation score 5
		XPNPEP2	7512	Downregulation score 8
Transcription_receptor-mediated HIF regulation	1.95×10^{-2}	*MTOR*	2475	Genetic score 4
		PTEN	5728	Genetic score 3
Serotonin modulation of dopamine release in nicotine addiction	2.24×10^{-2}	*PTEN*	5728	Genetic score 3
		CHRM1	1128	Downregulation score 8
Signal transduction_AKT signaling	2.34×10^{-2}	*MTOR*	2475	Genetic score 4
		PTEN	5728	Genetic score 3
cAMP/ Ca(2+)-dependent Insulin secretion	2.34×10^{-2}	*PLCE1*	51196	Genetic score 3
		RYR2	6262	Genetic score 3
Immune response_interleukin-4 signaling pathway	2.45×10^{-2}	*MTOR*	2475	Genetic score 4
		GATA3	2625	Downregulation score 6
Role of alpha-6/beta-4 integrins in carcinoma progression	2.55×10^{-2}	*MTOR*	2475	Genetic score 4
		EGF	1950	Downregulation score 10
G-protein signaling_regulation of cAMP levels by muscarinic acetylcholine receptor	2.55×10^{-2}	*PLCE1*	51196	Genetic score 3
		CHRM1	1128	Downregulation score 8
Development_PIP3 signaling in cardiac myocytes	2.77×10^{-2}	*MTOR*	2475	Genetic score 4
		PTEN	5728	Genetic score 3

Table 3. Statistically significant GeneGo pathway maps revealed by MetaCore pathway analysis (Continued)

Pathway	*P*-value	Involved genes		
		Genes	Entrez Gene ID	Multilayer-omics scoring (exome, methylome and transcriptome)
Some pathways of EMT in cancer cells	3.22×10^{-2}	*MTOR*	2475	Genetic score 4
		EGF	1950	Downregulation score 10
Development_beta-adrenergic receptors signaling *via* cAMP	3.34×10^{-2}	*RYR2*	6262	Genetic score 3
		TNNC1	7134	Downregulation score 5
Development_IGF-1 receptor signaling	3.34×10^{-2}	*MTOR*	2475	Genetic score 4
		PTEN	5728	Genetic score 3
Translation _regulation of EIF4F activity	3.45×10^{-2}	*MTOR*	2475	Genetic score 4
		EGF	1950	Downregulation score 10
G-protein signaling_RAP2B regulation pathway	3.81×10^{-2}	*PLCE1*	51196	Genetic score 3
DNA damage_DNA-damage-induced responses	4.87×10^{-2}	*ATM*	472	Genetic score 3

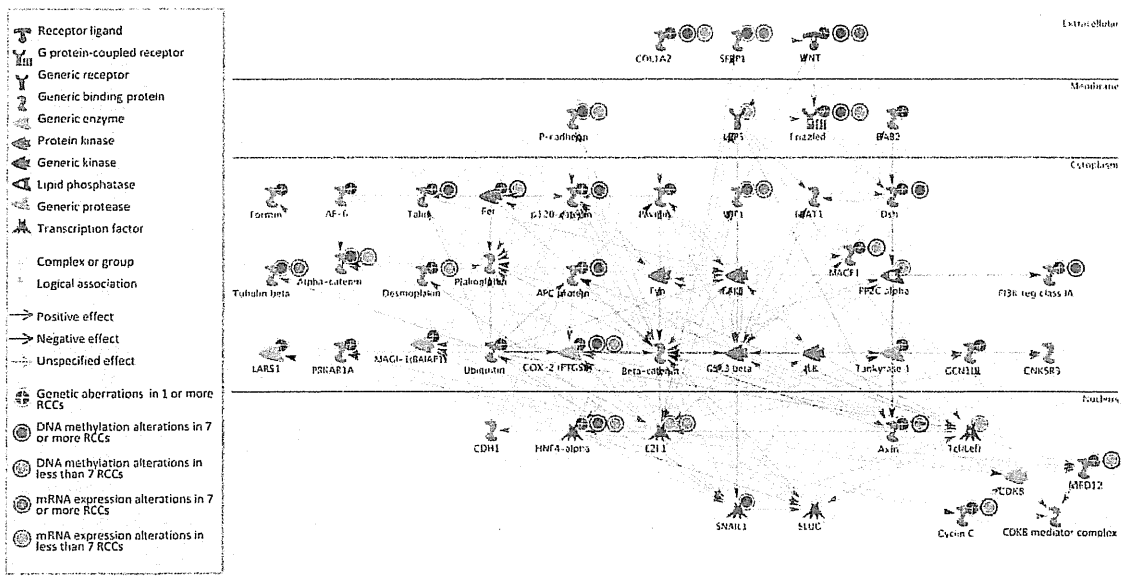

Figure 1. Genes for which a correlation with Wnt/β-catenin signaling was indicated by MetaCore pathway analysis. The numbers of genetic aberrations, DNA hyper- or hypo-methylation and/or increased or reduced mRNA expression (shown in Supporting Information Table S6) detected among the 67 examined RCCs are indicated schematically: legends are shown at the left of the panel. The 36 marked genes that showed genetic aberration, DNA methylation alterations and/or mRNA expression alterations in one or more RCCs were correlated with Wnt/β-catenin signaling.

to 29 RCCs for which transcriptome analysis was performed, mRNA expression levels of the targets genes of the Wnt/β-catenin signaling, such as *MYC*,[37] *MYCN*,[37] *IGF2*,[38] *POU5F1*,[39] *SOX9*,[40] *CYR61*,[41] *ENPP2*[42] and *MITF*,[43] tended to be higher in the 8 RCCs with mutations of any of the *GCN1L1*, *MED12*, *CCNC* and *MACF1* genes than in 21 RCCs without them (Supporting Information Table S10), indicating that such mutations may result in activation of Wnt/β-catenin signaling.

The downregulation score for the *SFRP1* gene was 6: reduced expression associated with DNA hypermethylation of *SFRP1* was frequent in clear cell RCCs. Members of the secreted frizzled-related protein (SFRP) family contain an N-terminal domain homologous to the cysteine-rich domain of the Wnt receptor Frizzled and lack a transmembrane region and the cytoplasmic domain required for transduction of signals into the cells.[44] This enables SFRPs to downregulate Wnt/β-catenin signaling by competing with Frizzled for Wnt binding *via* their cysteine-rich domain. Silencing of *SFRP1* due to DNA hypermethylation is known to result in activation of Wnt/β-catenin signaling.[44]

Since this study indicated possible alternative activation mechanisms (mutations of the *GCN1L1, MED12, CCNC* and *MACF1* genes and reduced expression of *SFRP1* due to DNA hypermethylation), we extensively examined Wnt/β-catenin signaling. MetaCore pathway analysis revealed that the 36 genes (marked in Fig. 1 and included in Supporting Information Table S6), which showed genetic aberration, DNA hypermethylation or hypomethylation and/or increased or reduced mRNA expression in one or more RCCs, are included in the Wnt/β-catenin signaling pathway. The present multilayer-omics analysis revealed that the Wnt/β-catenin signaling pathway may be of greater significance in renal carcinogenesis than was realized previously.

ERC2, which had a genetic aberration score of 4, is localized in presynaptic active zones and plays a critical role in neurotransmitter release.[45] Interaction between *ERC2* and the tandem PDZ protein syntenin-1, which is known to associate with many synaptic proteins, together with multimerization of *ERC2* both promote the localization of syntenin-1 at presynaptic *ERC2* clusters and contribute to the molecular organization of active zones.[45] Although the significance of *ERC2* in human cancers has remained unclear, frequent intragenic breaks in the *ERC2* gene indicated disruption of *ERC2* function in RCCs. In addition to recurrent genetic aberration, the present quantitative RT-PCR revealed frequent reduction of *ERC2* expression in clear cell RCCs relative to the corresponding N samples. Although frequent genetic and transcriptional inactivation of *ERC2* may be involved in renal carcinogenesis, further functional analysis of *ERC2* in RCCs is needed.

ABCA13 is a member of ATP-binding cassette sub-family A (*ABC1*) and a transmembrane transporter.[46] Xenobiotics, including anticancer drugs, are extensively metabolized by activation enzymes such as cytochromes *P450* and conjugation enzymes such as glutathione S-transferases or glucuronide transferases. Biotransformation represented by ABC transporters represents another important component of xenobiotic metabolism. In addition, ABC transporters play a crucial role in the development of resistance through efflux of anticancer agents from cancer cells.[46] The disease-free interval of patients with colorectal cancers treated by adjuvant chemotherapy is significantly shorter in patients with low *ABCA13* transcript levels.[47] In addition to recurrent genetic aberration (Table 1), the present quantitative RT-PCR revealed frequently reduced expression of *ABCA13* in RCCs relative to the corresponding N samples. Our findings suggest that it may be necessary to pay more attention to aberrations of *ABCA13* at both the genetic and expressional levels when deciding the indications for chemotherapy in patients with clear cell RCCs.

In Table 3 based on MetaCore pathway analysis, it is feasible that expression of *CLDN*s required for generating cation-selective paracellular channels[48] was reduced in clear cell RCCs, which lack the original absorptive function of the renal tubule. Moreover, *MTOR* mutations were highlighted as one of the major disrupters of multiple cell signaling during renal carcinogenesis: the *MTOR* gene participated in 10 (50%) of the 20 significant pathways in Table 3. The mammalian target of rapamycin (*mTOR*) encoded by the *MTOR* gene is a serine/threonine kinase that regulates cell growth, proliferation and autophagy.[49] *mTOR* inhibitors, such as rapamycin and its derivatives, are being introduced for targeted therapy of clear cell RCCs. Overactivation of *mTOR* is generally considered to be due to homozygous deletion of the *PTEN* tumor suppressor gene.[50] However, all 4 mutations of the *MTOR* gene detected in this cohort were located close to the kinase domain (data not shown) and may be activating mutations, as a previous *in vitro* study has suggested that mutations located close to the kinase domain activate the mutant form of *mTOR*.[50] In addition, all detected mutations of the *MTOR* gene showed a SIFT score of 0 and PolyPhen-2 scores of 0.998 or 0.999, strongly suggesting that all *MTOR* mutations affect protein function (Table 1 and Supporting Information Table S3). *MTOR* mutation may be a marker for predicting the sensitivity of clear cell RCCs to rapamycin therapy.

In summary, the present exome analysis has revealed frequent genetic aberrations of *GCN1L1, MED12, CCNC, MACF1, ERC2, ABCA13* and *MTOR* in clear cell RCCs. In addition to confirming the significance of aberrations of chromatin remodeling and histone modification-related proteins, the present multilayer-omics analysis has highlighted the significance of dysregulation of the Wnt/β-catenin signaling pathway including *CDK8* mediator function, as well as the need to pay closer attention to *MTOR* mutations, causing major disruption of cell signaling during renal carcinogenesis, in relation to chemosensitivity. Multilayer-omics analysis can be considered a powerful tool for revealing significant carcinogenetic pathways in human cancers.

References

1. Ljungberg B, Campbell SC, Choi HY, et al. The epidemiology of renal cell carcinoma. *Eur Urol* 2011;60: 615–21.
2. Dalgliesh GL, Furge K, Greenman C, et al. Systematic sequencing of renal carcinoma reveals inactivation of histone modifying genes. *Nature* 2010;463:360–3.
3. van Haaften G, Dalgliesh GL, Davies H, et al. Somatic mutations of the histone H3K27 demethylase gene UTX in human cancer. *Nat Genet* 2009;41:521–3.

4. Varela I, Tarpey P, Raine K, et al. Exome sequencing identifies frequent mutation of the SWI/SNF complex gene PBRM1 in renal carcinoma. *Nature* 2011;469:539–42.
5. Baldewijns MM, van Vlodrop IJ, Vermeulen PB, et al. VHL and HIF signaling in renal cell carcinogenesis. *J Pathol* 2010;221:125–38.
6. Guo G, Gui Y, Gao S, et al. Frequent mutations of genes encoding ubiquitin-mediated proteolysis pathway components in clear cell renal cell carcinoma. *Nat Genet* 2012;44:17–9.
7. Baylin SB, Jones PA. A decade of exploring the cancer epigenome - biological and translational implications. *Nat Rev Cancer* 2011;11:726–34.
8. Kanai, Y. Genome-wide DNA methylation profiles in precancerous conditions and cancers. *Cancer Sci* 2010;101:36–45.
9. Arai E, Ushijima S, Fujimoto H, et al. Genome-wide DNA methylation profiles in both precancerous conditions and clear cell renal cell carcinomas are correlated with malignant potential and patient outcome. *Carcinogenesis* 2009;30:214–21.
10. Arai E, Kanai Y, Ushijima S, et al. Regional DNA hypermethylation and DNA methyltransferase (DNMT) 1 protein overexpression in both renal tumors and corresponding nontumorous renal tissues. *Int J Cancer* 2006;119:288–96.
11. Arai E, Chiku S, Mori T, et al. Single-CpG-resolution methylome analysis identifies clinicopathologically aggressive CpG island methylator phenotype clear cell renal cell carcinomas. *Carcinogenesis* 2012;33:1487–93.
12. Sato Y, Yoshizato T, Shiraishi Y, et al. Integrated molecular analysis of clear-cell renal cell carcinoma. *Nat Genet* 2013;45:860–7.
13. Eble JN, Togashi K, Pisani P. Renal cell carcinoma. World Health Organization classification of tumours. Pathology and genetics. Tumours of the urinary system and male genital organs. Lyon: IARC Press, 2004. 10–43.
14. Fuhrman SA, Lasky LC, Limas, C. Prognostic significance of morphologic parameters in renal cell carcinoma. *Am J Surg Pathol* 1982;6:655–63.
15. Sobin LH, Gospodarowicz MK, Wittekind C, eds. International Union Against Cancer (UICC). TNM classification of malignant tumors, 7th edn. New York: Wiley, 2009.
16. Li H, Durbin R. Fast and accurate long-read alignment with Burrows-Wheeler transform. *Bioinformatics* 2010;26:589–95.
17. Ye K, Schulz MH, Long Q, et al. Pindel: a pattern growth approach to detect break points of large deletions and medium sized insertions from paired-end short reads. *Bioinformatics* 2009;25: 2865–71.
18. Wang L, Tsutsumi S, Kawaguchi T, et al. Whole-exome sequencing of human pancreatic cancers and characterization of genomic instability caused by MLH1 haploinsufficiency and complete deficiency. *Genome Res* 2012;22:208–19.
19. Ng PC, Henikoff S. Accounting for human polymorphisms predicted to affect protein function. *Genome Res* 2002;12:436–46.
20. Hicks S, Wheeler DA, Plon SE, et al. Prediction of missense mutation functionality depends on both the algorithm and sequence alignment employed. *Hum Mutat* 2011;32:661–8.
21. Sim NL, Kumar P, Hu J, et al. SIFT web server: predicting effects of amino acid substitutions on proteins. *Nucleic Acids Res* 2012;40:W452–7.
22. Van Loo P, Nordgard SH, Lingjærde OC, et al. Allele-specific copy number analysis of tumors. *Proc Natl Acad Sci USA* 2010;107:16910–5.
23. Li A, Liu Z, Lezon-Geyda K, et al. GPHMM: an integrated hidden Markov model for identification of copy number alteration and loss of heterozygosity in complex tumor samples using whole genome SNP arrays. *Nucleic Acids Res* 2011;39: 4928–41.
24. Nagashio R, Arai E, Ojima H, et al. Carcinogenetic risk estimation based on quantification of DNA methylation levels in liver tissue at the precancerous stage. *Int J Cancer* 2011;129: 1170–9.
25. Firestein R, Hahn WC. Revving the Throttle on an oncogene: CDK8 takes the driver seat. *Cancer Res* 2009;69:7899–901.
26. Firestein R, Bass AJ, Kim SY, et al. CDK8 is a colorectal cancer oncogene that regulates beta-catenin activity. *Nature* 2008;455:547–51.
27. He SB, Yuan Y, Wang L, et al. Effects of cyclin-dependent kinase 8 specific siRNA on the proliferation and apoptosis of colon cancer cells. *J Exp Clin Cancer Res* 2011;30:109.
28. Seo JO, Han SI, Lim SC. Role of CDK8 and beta-catenin in colorectal adenocarcinoma. *Oncol Rep* 2010;24:285–91.
29. Carrera I, Janody F, Leeds N, et al. Pygopus activates Wingless target gene transcription through the mediator complex subunits Med12 and Med13. *Proc Natl Acad Sci USA* 2008;105:6644–9.
30. Yoda A, Kouike H, Okano H, et al. Components of the transcriptional mediator complex are required for asymmetric cell division in C. elegans. *Development* 2005;132:1885–93.
31. Mäkinen N, Mehine M, Tolvanen J, et al. MED12, the mediator complex subunit 12 gene, is mutated at high frequency in uterine leiomyomas. *Science* 2011;334:252–5.
32. Jackson A, Carrara P, Duke V, et al. Deletion of 6q16-q21 in human lymphoid malignancies: a mapping and deletion analysis. *Cancer Res* 2000; 60:2775–9.
33. Ohata N, Ito S, Yoshida A, et al. Highly frequent allelic loss of chromosome 6q16-23 in osteosarcoma: involvement of cyclin C in osteosarcoma. *Int J Mol Med* 2006;18:1153–8.
34. Banumathy G, Cairns P. Signaling pathways in renal cell carcinoma. *Cancer Biol Ther* 2010;10: 658–64.
35. Andrade MA, Petosa C, O'Donoghue SI, et al. Comparison of ARM and HEAT protein repeats. *J Mol Biol* 2001;309:1–18.
36. Chen HJ, Lin CM, Lin CS, et al. The role of microtubule actin cross-linking factor 1 (MACF1) in the Wnt signaling pathway. *Genes Dev* 2006;20:1933–45.
37. Karim R, Tse G, Putti T, et al. The significance of the Wnt pathway in the pathology of human cancers. *Pathology* 2004;36:120–8.
38. Heaton JH, Wood MA, Kim AC, et al. Progression to adrenocortical tumorigenesis in mice and humans through insulin-like growth factor 2 and β-catenin. *Am J Pathol* 2012;181:1017–33.
39. Li J, Li J, Chen B. Oct4 was a novel target of Wnt signaling pathway. *Mol Cell Biochem* 2012; 362:233–40.
40. Blache P, van de Wetering M, Duluc I, et al. SOX9 is an intestine crypt transcription factor, is regulated by the Wnt pathway, and represses the CDX2 and MUC2 genes. *J Cell Biol* 2004;166:37–47.
41. Li ZQ, Ding W, Sun SJ, et al. Cyr61/CCN1 is regulated by Wnt/β-catenin signaling and plays an important role in the progression of hepatocellular carcinoma. *PLoS One* 2012;7:e35754.
42. Zirn B, Samans B, Wittmann S, et al. Target genes of the WNT/beta-catenin pathway in Wilms tumors. *Genes Chromosomes Cancer* 2006; 45:565–74.
43. Syed DN, Afaq F, Maddodi N, et al. Inhibition of human melanoma cell growth by the dietary flavonoid fisetin is associated with disruption of Wnt/β-catenin signaling and decreased Mitf levels. *J Invest Dermatol* 2011;131:1291–9.
44. Suzuki H, Watkins DN, Jair KW, et al. Epigenetic inactivation of SFRP genes allows constitutive WNT signaling in colorectal cancer. *Nat Genet* 2004;36:417–22.
45. Ko J, Yoon C, Piccoli G, et al. Organization of the presynaptic active zone by ERC2/CAST1-dependent clustering of the tandem PDZ protein syntenin-1. *J Neurosci* 2006;26:963–70.
46. Cole SP, Bhardwaj G, Gerlach JH, et al. Overexpression of a transporter gene in a multidrug-resistant human lung cancer cell line. *Science* 1992;258:1650–4.
47. Hlavata I, Mohelnikova-Duchonova B, Vaclavikova R, et al. The role of ABC transporters in progression and clinical outcome of colorectal cancer. *Mutagenesis* 2012;27:187–96.
48. Angelow S, El-Husseini R, Kanzawa SA, et al. Renal localization and function of the tight junction protein, claudin-19. *Am J Physiol Renal Physiol* 2007;293:166–77.
49. Populo H, Lopes JM, Soares P. The mTOR signalling pathway in human cancer. *Int J Mol Sci* 2012;13:1886–918.
50. Sato T, Nakashima A, Guo L, et al. Single amino-acid changes that confer constitutive activation of mTOR are discovered in human cancer. *Oncogene* 2010;29:2746–52.

Jpn J Clin Oncol 2014;44(2)191–194
doi:10.1093/jjco/hyt192
Advance Access Publication 13 December 2013

Secondary Osteosarcoma Developing 10 Years after Chemoradiotherapy for Non-small-cell Lung Cancer

Shigehiro Yagishita[1], Hidehito Horinouchi[1,*], Takashi Yorozu[2], Satoru Kitazono[1], Hidenori Mizugaki[1], Shintaro Kanda[1], Yutaka Fujiwara[1], Hiroshi Nokihara[1], Noboru Yamamoto[1], Taisuke Mori[2], Koji Tsuta[2], Minako Sumi[3] and Tomohide Tamura[1]

[1]Division of Thoracic Oncology, National Cancer Center Hospital, Tokyo, [2]Division of Pathology, National Cancer Center Hospital, Tokyo and [3]Division of Radiation Oncology, National Cancer Center Hospital, Tokyo, Japan

*For reprints and all correspondence: Hidehito Horinouchi, Division of Thoracic Oncology, National Cancer Center Hospital, Tsukiji 5-1-1, Chuo-ku, Tokyo 1040045, Japan. E-mail: hhorinou@ncc.go.jp

Received July 30, 2013; accepted November 12, 2013

A 53-year-old female patient was admitted with pain and a progressively enlarging mass in the right upper chest. Chest computed tomography revealed a mass lesion in the region of the right upper ribs. Ten years prior to this admission, the patient had undergone right lobectomy for lung adenocarcinoma. One year after the surgery, follow-up computed tomography had revealed tumor recurrence in the mediastinal and supraclavicular lymph nodes, and the patient had been treated by chemoradiotherapy. Thereafter, regular follow-up had revealed no evidence of recurrence of the non-small-cell lung cancer. Histopathological findings revealed proliferation of spindle-shaped malignant tumor cells in a background of osteoid, consistent with the diagnosis of osteosarcoma. The location of the tumor was consistent with the radiation field. Based on the clinicopathological findings, the patient was diagnosed as having secondary osteosarcoma occurring as a result of the chemoradiotherapy administered previously for the recurrent non-small-cell lung cancer. Unfortunately, the patient died of rapid progression of the osteosarcoma within a week of admission to the hospital. The autopsy revealed contiguous invasion by the tumor of the heart, with massive thrombus formation. The peripheral pulmonary arteries were diffusely occluded by metastatic tumors. Our case serves to highlight the risk of development of secondary sarcoma as a life-threatening late complication after chemoradiotherapy for locally advanced non-small-cell lung cancer, even after complete cure of the primary tumor.

Key words: chemoradiotherapy – non-small-cell lung cancer – osteosarcoma – secondary sarcoma

CASE REPORT

A 53-year-old female, a never-smoker, presented with pain and a progressively enlarging mass on the right upper chest. Computed tomography (CT) revealed a mass measuring 110 mm in diameter in the region of the first to third ribs, which showed direct invasion of the superior vena cava. Positron emission tomography-CT with [18F] fluorodeoxyglucose showed a maximum standard uptake value of 13.1 in the right chest wall mass (Fig. 1).

Ten years prior to this admission, the patient had undergone right upper and middle bi-lobectomy for the diagnosis of non-small-cell lung cancer (NSCLC). Histopathological examination of the resected specimens had shown synchronous double primary disease, consisting of an invasive adenocarcinoma with pulmonary metastasis (T4N2M0) in the right upper lobe and a non-invasive adenocarcinoma (T1N0M0) in the right middle lobe. The patient did not receive postoperative therapy because there was no result of confirmatory